


## Monitoring of winter wheat growth in categories of frost damage and production potential using SAR and optical images\*\*

Miloš Láznička<sup>1</sup>, Lukáš Tůma<sup>1</sup>, Věra Vandírková<sup>2</sup>, Marie Wohlmuthová<sup>3</sup>, Martin Kotek<sup>2</sup>,  
František Kumhála<sup>1</sup>, Jitka Kumhálová<sup>2</sup> \*

<sup>1</sup>Department of Agricultural Machines, Czech University of Life Sciences Prague,

<sup>2</sup>Department of Vehicles and Ground Transport, Czech University of Life Sciences Prague,

<sup>3</sup>Department of Mathematics, Czech University of Life Sciences Prague,  
Kamýcká 129, 165 21 Prague 6-Suchdol, Czech Republic

Received August 12, 2024; accepted November 8, 2024

**Abstract.** Remote sensing plays an increasingly important role in agriculture, especially in monitoring the quality of agricultural crops. Optical sensing is often limited in Central Europe due to cloud cover; therefore, synthetic aperture radar data is increasingly being used. However, synthetic aperture radar data is limited by more difficult interpretation mainly due to the influence of speckles. For this reason, its use is often limited to larger territorial units and field blocks. The main aim of this study therefore was to verify the possibility of using satellite synthetic aperture radar images to assess the within-field variability of winter wheat. The lowest radar vegetation index values corresponded to the area of the lowest production potential and the greatest damage to the stand. Also for VH and VV polarizations, the highest values corresponded to the area of the lowest stand quality. Qualitative changes in the stand across the zones defined by frost damage and production potential were assessed with the help of the logistic regression model with resampled data for 10, 50, and 100 m pixel size. The best correlation coefficients were achieved at a spatial resolution of 50 m for both options. The F-score still yielded a promising result ranging from 0.588 to 0.634 for frost damage categories. The regression model of the production potential performed slightly better in terms of the F-score, recall, and precision at higher resolutions. It was proved that modern statistical methods could be used to reduce problems associated with speckles of radar images for practical purposes.

**Keywords:** Sentinel-1, polarizations, spring frost, field variability, logistic regression model

### 1. INTRODUCTION

Winter wheat (*Triticum spp.*) is the most frequently grown cereal in the Czech Republic, covering approximately 32% of arable land (ČSÚ, 2021). The yield of agricultural crops is influenced by many factors, including topography, soil properties, field management, fertilizing, and meteorological conditions during the growing season (Kumhálová *et al.*, 2011; Madaras *et al.*, 2018; Balážová *et al.*, 2021; Rataj *et al.*, 2022). Oerke (1994), Thielert (2006), and Kajla *et al.* (2015) investigated the causes of crop yield losses. According to their studies, abiotic factors account for 50% (of which 20% are high temperatures, 7% low temperatures, 9% drought, 10% salinity, and the remaining 4% are other abiotic stressors. Depending on the local habitat conditions and geographical area, a cultivar with sufficient resistance to biotic and abiotic influences should be usually chosen (Jelínek *et al.*, 2020). Weather extremes, which can be a consequence of climate change, are currently a significant problem; therefore, winter wheat cultivars adapted to central European climatic regions also with ability to face local adverse biotic and abiotic influences were registered from 1976 to 2009 (Šíp *et al.*, 2011). Rising average temperature is a sign of climate change and causes

\*Corresponding author e-mail: kumhalova@tf.czu.cz

\*\*This work was supported by the Ministry of Agriculture of the Czech Republic, research project NAZV QK 22010014; and Internal Grant of Faculty of Engineering CZU 2021:31150/1312/3113.



a recurring frequency of weather extremes affecting agricultural production and yield (Fuglie, 2021); in the periods 1850-1900 and 2006-2015 alone, the average surface temperature increased by 1.53 °C (“Special Report on Climate Change and Land – IPCC site,” n.d.) (IPCC, 2020). One of the impacts of the increased average temperature indicates a lower risk of affecting crop growth at low temperatures. On the other hand, the risk of frost damage to crop may not be proportionally reduced by the interaction on the change in ambient temperature (Rapacz *et al.*, 2014). Irregular frosty days lead to an increased risk of frost damage to crops, especially in an area where the vegetation is not covered with snow due to a decrease in snow cover (Dalmannsdottir *et al.*, 2017). Currently, many wheat cultivars resistant to extreme weather have been bred and are commonly sown around the world. However, because of extreme weather changes in areas where spring frosts may appear, damage to the crop stand and subsequent loss of yields may occur (Zhong *et al.*, 2008). Challinor *et al.* (2005) found that temperature is one of the main factors for crop yield estimation and crop production. Various crop models are currently used to optimize production and predict crop growth, but their major drawback may be their limited ability to predict climatic extremes and the frequent requirement of a lot of input data (Sánchez *et al.*, 2014; Rapacz *et al.*, 2022; Barlow *et al.*, 2015; Persson *et al.*, 2017). On the other hand, the damage to the crop stand can be monitored during the entire growth in individual phenological stages and using noninvasive methods. The information can also be converted into a quantitative form to estimate the economic damage. Each plant organ is sensitive to frost to a different degree. The most important organ of winter wheat is undoubtedly the crown tissue (Persson *et al.*, 2017). In the case of spring frosts or extreme temperature during the winter, it enables the regeneration of other plant organs that are damaged (Fowler *et al.*, 1999). Due to its high sensitivity to frost, it is very important to monitor the vitality and health of the crown tissue. Extensive information about its condition and phenology can be obtained using remote sensing (Vaghela *et al.*, 2020).

Remote sensing offers a contactless way of monitoring crops. With the development of modern technologies in plant production (including satellite images with high spatial and temporal resolution), digital information from sensors is increasingly being used for agrotechnical purposes (Atzberger, 2013; Nasrallah *et al.*, 2018). Especially, optical remote sensing is often used for assessment, inventory, and modeling purposes with its tradition of more than a hundred years. A significant development in this field was mainly the launch of Landsat satellites of the U.S. Geological Survey (USGS) and NASA in 1972 (Landsat Science, (n.d.), 2023) and the Copernicus program satellites of the European Space Agency (ESA) in 2014 into orbit (ESA – Copernicus (n.d.), 2023). Although optical data is a valuable source of information, it has its limitations.

One of them is limitations caused by weather conditions, such as frequent cloud cover, which is a significant problem over the area of the Czech Republic, and the limited availability of cloud-free images during the growing season (Domínguez *et al.*, 2015). However, these limitations can be reduced by the use of microwave remote sensing, *i.e.* images from Sentinel-1. As reported by Kim *et al.* (2012), Malenovský *et al.* (2012), Fieuzal *et al.* (2013) and Jin *et al.* (2015), the great advantage of the microwave part of the spectrum is that it can penetrate through clouds and thus data can be obtained regardless of the time of day.

Growth prediction and periodicity models in the crop life cycle with emphasis on the phenology and health status of the crops in the field or individual parts of the field are crucial for crop management. The crop life cycle can fluctuate according to weather conditions in seasons and cultivars. Domínguez *et al.* (2015) developed predictive models for winter wheat and winter oilseed rape for local field conditions and cultivars. They used the normalized difference vegetation index (NDVI, Rouse *et al.*, 1973) for its simulation and easy interpretation. On the other hand, the use of time series from optical data requires a large data set with homogenous atmospheric conditions, which can be limited due to frequent cloud cover. It is also necessary to focus on individual spectral bands. Jelínek *et al.* (2020) considered the use of spectral bands B8 and B8A of Sentinel 2 images for calculating NDVI and their suitability for evaluating winter wheat varieties. During the last years, many studies have been published concerning yield potential and its modeling. Basic rules about this issue (*e.g.* photosynthesis, water uptake, nutrition) were already set by Evans (1996). Yield potential is primarily defined as the relative yield of a variety, which is already adapted and grown in conditions with non-limiting water and nutrient access and biotic stresses, also effectively controlled. However, as pointed out by Guilpart *et al.* (2017), the definition of crop yield is not static in the real world and evolves based on the intensity of the cropping system. Because it was necessary to transfer the models to a clear visualization and thus improve the interpretation of the variability of the annual yield map, Maphanyane (2017) published a concept of a normalized yield frequency map. Such a model converts absolute yield into relative yield and thus identifies places with higher or lower production capacity.

Synthetic aperture radar (SAR) data and radar backscatter in general can serve as an alternative to optical data for monitoring the growth of various agricultural crops (Kumar Sahadevan *et al.*, 2013; Mandal *et al.*, 2020; Kaplan *et al.*, 2021; de Blas *et al.*, 2021; Saad El Imanni *et al.*, 2022 and others). The authors often combine optical and radar satellite data for wheat monitoring, as in Saad El Imanni *et al.* (2022). However, as it turned out in the study by Tůma *et al.* (2022), a major problem in the usability and interpretation of Sentinel-1 radar images may be the backscatter anisotropy caused by the different

incidence and azimuthal angles. For this reason, it is necessary to choose at least the same orbit for all images in the time series. Speckle filtering is also one of the necessary procedures for increasing image quality by reducing speckle (Filipponi, 2019) and plays a significant role for the final visualization and interpretation of results.

In addition to the Radar vegetation index (RVI, Charbonneau, 2005), dual polarizations are also very often used in agriculture. The signal from the cross-polarized channels (HV and VH) is sensitive to structural parameters, where the resulting value is high for multiple backscatters, while the resulting value is low for a single backscatter, e.g. from bare soil. On the other hand, co-polarized channels (HH or VV) are more sensitive to water content or surface roughness (soil, vegetation) (Moreira *et al.*, 2013; Harfenmeister *et al.*, 2019). Alternative equations using VH and VV channels have been proposed for dual-polarized SAR sensors, such as Sentinel-1 (Trudel *et al.*, 2012; Mandal *et al.*, 2020).

Since SAR images are not affected by clouds, they can supplement information on the canopy if properly processed. Just as the commonly used optical spectral indices or spectral bands can predict and quite clearly describe the state, structure, and vitality of crops, information from SAR can also contribute to supplementing and completing information on the structural parameters of biomass, water content, or surface roughness (growth phases).

As is clear from the previous text, the advantageous combination of optical and microwave remote sensing, or remote sensing in the pure microwave spectrum, is increasingly being used to monitor the growth and condition of agricultural crops. However, current publications show that this monitoring is most often used at the level of entire plots of land. For example, Mandal *et al.* (2020) used Sentinel-1 SAR data to monitor the growth of canola, soybean, and wheat. Subsequently, Kaplan *et al.* (2021) used Sentinel-1 images for monitoring processing potatoes and cotton, de Blas *et al.* (2021) predicted crop biophysical variables from Radarsat-2 imagery, and Saad El Imanni *et al.* (2022) investigated the efficiency of Sentinel-1 and Sentinel-2 data to study wheat phenological stages. Recently, Bao *et al.* (2023) extracted vegetation descriptors from Sentinel-1 SAR data for wheat, canola, corn, and soybeans. Crop NDVI time series construction by fusing Sentinel-1 and 2 was also discussed for corn and soybean by Chen *et al.* (2023), while Qu *et al.* (2023) monitored corn lodging based on Sentinel-1 images. Gao *et al.* (2023) used a combination of Sentinel-1 and 2 images for large scale rice mapping, and finally, Ya'nan *et al.* (2024) used a combination of data from Sentinel-1 and 2 for surface soil moisture mapping over agricultural regions.

However, there are also studies that try to capture variability at the field scale. For example, Hernández *et al.* (2022) used a combination of Landsat-8/OLI optical images and Sentinel-1 radar images to map wheat plants stressed

by a soil aluminum effect, and Lapaz Oliveira *et al.* (2023) used a combination of data from Sentinel-1 and 2 to create empirical models of remotely sensed corn nitrogen status within field during the vegetative period. Nevertheless, we have no information that only radar data itself was used to evaluate the within-field variability.

These recently published studies encouraged us to try to use pure radar satellite imagery to assess the within-field variability of winter wheat frost damage or its production potential. The first case happens increasingly often in the conditions of the Czech Republic in the early spring season in connection with climate change. We have no information that these issues were resolved in the past. That is why the novelty of this paper lies primarily in the fact that we have attempted to address this challenge.

Therefore, the main objective of this study was to verify the possibility of using satellite SAR images to assess the variability of vegetation within one plot. It was assessed whether it was possible to capture the qualitative changes in the winter wheat stand across the defined zones based on (1) frost damage and (2) production potential maps using the potential of SAR Sentinel-1 images.

## 2. MATERIALS AND METHODS

### 2.1. Study area

For the purposes of this experiment, four agricultural fields with winter wheat were selected, partially damaged by spring frosts and secondarily by photooxidative radiation in April 2020. The study area was located near Lišany village (50.1563328N, 13.7396500E) in the Czech Republic, belonging to the Agricultural Company Lupofyt s.r.o. The total area of the monitored plots was 67.2 ha with 350.30 m a.s.l. average elevation and 3.3% slope. An overview of the topographic parameters for individual monitored fields is given in Table 1. Topographic attributes, such as slope and topography wetness index (TWI), were derived from the Digital Terrain Model of the Czech Republic of the 5th Generation (DMR5G). Data were processed according to methodology described in Kumhálová *et al.* (2013, 2014) and Rataj *et al.* (2022).

**Table 1.** Topographic attributes derived from the digital terrain model of the Czech Republic of the 5th generation (DMR5G)

Name	Area (ha)	Average elevation (m) a.s.l.	Slope (°)	TWI	Aspect (°)
NK	19.45	360.08	4.12	7.01	209.14
PS	7.19	335.24	1.89	7.68	194.20
PV	21.60	353.31	5.22	6.57	260.66
ZTC	18.96	349.02	2.91	7.33	246.94

The soil of the monitored fields belongs to eutrophic cambium soils and, in terms of soil particle grain size, mainly to loamy soils (ČGS, 2023). The conventional arable soil tillage technology (plowing) was used on the experimental plots.

Weather conditions, *i.e.* data on total daily precipitation as well as average daily and minimum temperatures in the main vegetation season 2020 provided by the official hydro-meteorological station Heřmanov in district Rakovník, are shown in Figure 1. In terms of climatic conditions, the area of interest is located in a moderately warm area, where the typical summer is reasonable with 10-20 summer days, moderately warm with an average temperature of 13-15°C and moderately humid with precipitation of 200-400 mm and 100-140 days with precipitation greater than 1 mm per day. According to the characteristics, winter is normally long with 50-60 icy days, slightly cold with an average temperature of -2 to -3°C, precipitation of 200-400 mm, and a snow cover duration of 50-80 days. The transition period (spring, autumn) is reasonably long with 140-160 frost days, a cool spring with an average temperature of 5-7°C, and a slightly warm autumn with an average temperature of 6-8°C (WMS – Climatic regions of the Czech Republic: <https://micka.cenia.cz/record/basic/4e64bc59-65b0-4475-aae2-06a8c0a80138>, 2024).

The crop rotation during the previous years was based on changing winter rape and winter wheat as the main production crops.

## 2.2. Yield data

Combine harvester Claas Lexion 750 Terra Trac was used for yield measurements. This machine was equipped with a yield monitor and a DGPS receiver. The EGNOS correction ensured the accuracy of this system ( $\pm 0.1-0.3$  m in horizontal and  $\pm 0.2-0.6$  m in vertical direction). The yield data were saved every 1 s with coordinates to the external memory. The yield data were processed with a basic statistical method in order to eliminate errors of the yield measurement system. The yield data sets were then inter-

polated to kriging maps using experimental variograms and common procedures. The method is described in detail in Kumhálová *et al.* (2011).

## 2.3. Remote sensing data

Sentinel-1 A/B SAR and Sentinel 2A/B optical satellite images for the main vegetation season 2020 (see Table 2) were downloaded from the Copernicus Open Access Hub (<https://scihub.copernicus.eu/>). Images from the Sentinel 2 satellite were used only for the purpose to evaluate the results obtained from radar data processing. Sentinel 2 images in the level of Bottom of Atmosphere (BOA) reflectance L2A were resampled to 10 m spatial resolution with the help of SW ENVI 5.5 (Excelis, Inv. Mc Lean, USA) or SNAP 6.0.4 (ESA, <http://step.esa.int/main/>). SAR data were downloaded for the same relative orbit 44 according to Tůma *et al.* (2022) recommendation to maintain the same properties of the images. SAR data processing consisted of several steps as follows: radiometric calibration, multi-temporal speckle filtering with using Lee sigma filter, and range-doppler terrain correction. Table 3 shows the vegetation indices and variables calculated and evaluated for the purpose of this study.

In SW QGIS (version 7.8.3), the centroids of the raster pixels inside the monitored plots were created, exported from optical satellite images (basically at a spatial resolution of 10 m). The centroids were then converted to text format and uploaded via the “Pin manager” tool to SW SNAP. Based on these points, variables, mentioned in Table 3, were quantified for each pixel of the given plots, which served as the basic data source for statistical analysis. Topographic attributes (Slope and TWI) and crop yield were then considered for advanced statistical analysis. Pixels were resampled to the spatial resolution 50 and 100 m with the aim to improve the information of raster data regarding to speckle filtering during the SAR data processing. These data sets were also taken to the advanced statistical analysis.

**Table 2.** Optical and SAR satellite images available for the main vegetation season for 2020

Satellite	Dates of images
Sentinel 1 SAR	22.3., 28.3., 3.4., 9.4., 21.4., 9.5., 15.5., 21.5., 2.6., 14.6., 20.6.
Sentinel 2 MSI	24.3., 8.4., 18.4., 23.4., 28.4., 8.5., 18.5., 2.6., 27.6.

**Table 3.** Vegetation indices and variables calculated in this study

Variables	Equation / property	Used for
Normalized difference vegetation index (NDVI)	$(\text{NIR}-\text{RED}) / (\text{NIR}+\text{RED})$	Structure, vigor, health of vegetation
Radar vegetation index (RVI)	$(4\sigma_{\text{VH}}) / (\sigma_{\text{VV}} + \sigma_{\text{VH}})$	Structure, moisture content
B8 (NIR) band of Sentinel 2 image	0.842 nm	Quality of cellular structure in crop tissue
VV polarization	co-polarized backscatter	Vertical structure of crops (height), moisture
VH polarization	cross-polarized backscatter	Crop volume, moisture

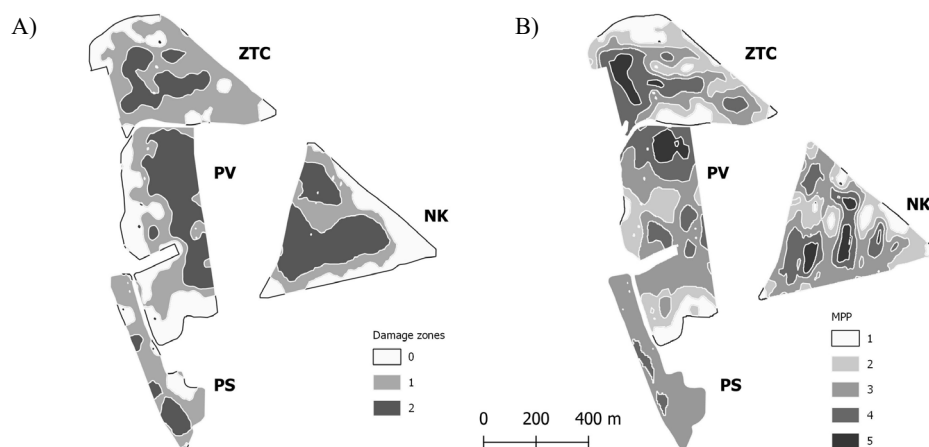


**Fig. 2.** Damage zones A) where: 0 – damaged wheat stands, 1 – medium vigor, 2 – best vigor and map of production potential (MPP); B) where: 1 – the lowest, 5 – the highest.

All the data were evaluated inside the individual categories derived from “production potential maps (MPP)” and “damage zones”. The damage zones of the wheat stand were determined based on the resulting yield data, which, according to the previous analysis and personal communication with an agronomist, corresponded to the degree of freezing of the wheat stand at the beginning of the main growing season. The winter wheat stands were visually monitored by an agronomist, who checked the individual fields and assessed the degree and extent of their damage. Three basic levels of damage were determined (Fig. 2) where: Category 0 – damaged wheat stands; Category 1 – medium vigor; Category 2 – best vigor. The production potential maps were derived according to common procedures mentioned *e.g.* in Jelínek *et al.* (2020) as the calculation of “yield frequency map” expressed in percentage as the level of average productivity of surveyed plots in five categories (Fig. 2). The information about the size of the individual damage zones and MPP categories is given in Tables 4 and 5.

#### 2.4. Data analysis

Data analysis was performed with resampled data for 10, 50, and 100 m pixel size with the aim to reduce the effect of speckles on the resulting analysis. The Python programming language with relevant libraries (Pandas, Scikit-Learn and Matplotlib) was utilized for data wrangling, statistical analysis, statistical model building, and performance measurements. The first step dealt with the merging data from the entire vegetation season together to one dataset. The number of samples was  $n = 6219$  for 10 m,  $n = 2860$  for 50 m, and  $n = 744$  for 100 m. However, in the case of logistic regression model training, the total number of initial training points was much higher, a total of 83619. It should be considered that several images (NDVI and RVI in several terms) were obtained from each sampling point of 10 x 10 m, not just one. Each of these images is then

**Table 4.** Area (ha) of damage zones, where 0 – damaged stands, 1 – medium vigor, 2 – best vigor

Field / Damage zones	0	1	2	Total area (ha)
NK	5.17	5.63	8.65	19.45
PS	1.19	4.44	1.56	7.19
PV	6.98	6.43	8.19	21.60
ZTC	3.29	11.48	4.19	18.96
Total area (ha)	16.63	28.98	24.59	67.20

**Table 5.** Area (ha) of map of production potential (MPP) categories, where 1 – the lowest, 5 – the highest

Field / MPP categories	1	2	3	4	5	Total area (ha)
NK	1.52	4.53	7.84	4.33	1.23	19.45
PS			6.54	0.65		7.19
PV	1.86	4.84	8.95	4.70	1.25	21.60
ZTC	3.25	5.17	4.75	4.57	1.22	18.96
Total area (ha)	6.63	14.54	28.08	14.25	3.70	67.20

a training point. After these initial data wrangling steps, the basic statistics was performed – correlation matrix and scatter matrices between zones of production potential (five zones) and other variables. Subsequently, the logistic regression model was built with three damage zones, TWI, Crop Yield, Slope, VV and VH polarization as explanatory variables and five zones of production potential as the dependent variable with a test data size of 0.3 for all the resolution variants. Finally, the confusion matrix, F-score, recall, and precision of the test were used for performance measurement. The reason for using the logistic regression

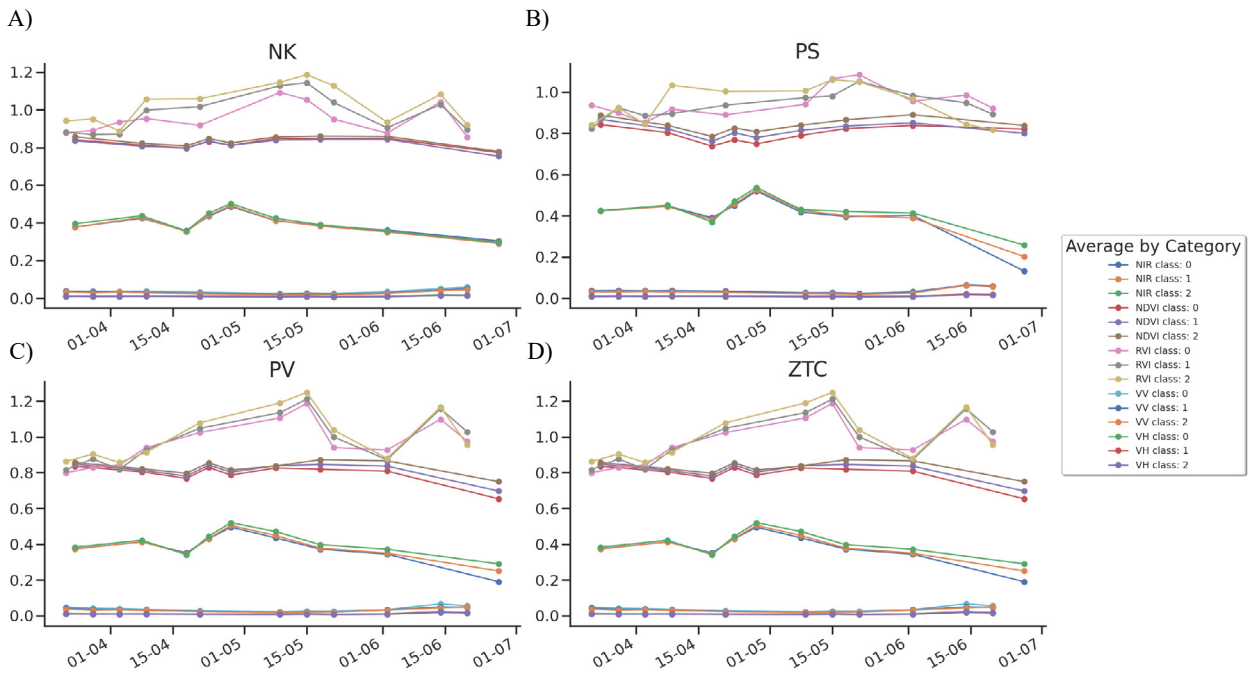


**Fig. 3.** Average values of three damage zones on the four monitored winter wheat plots: NK (A), PS (B), PV (C), ZTC (D) for selected variables during the main vegetation season 2020 (date on the “x” axis).

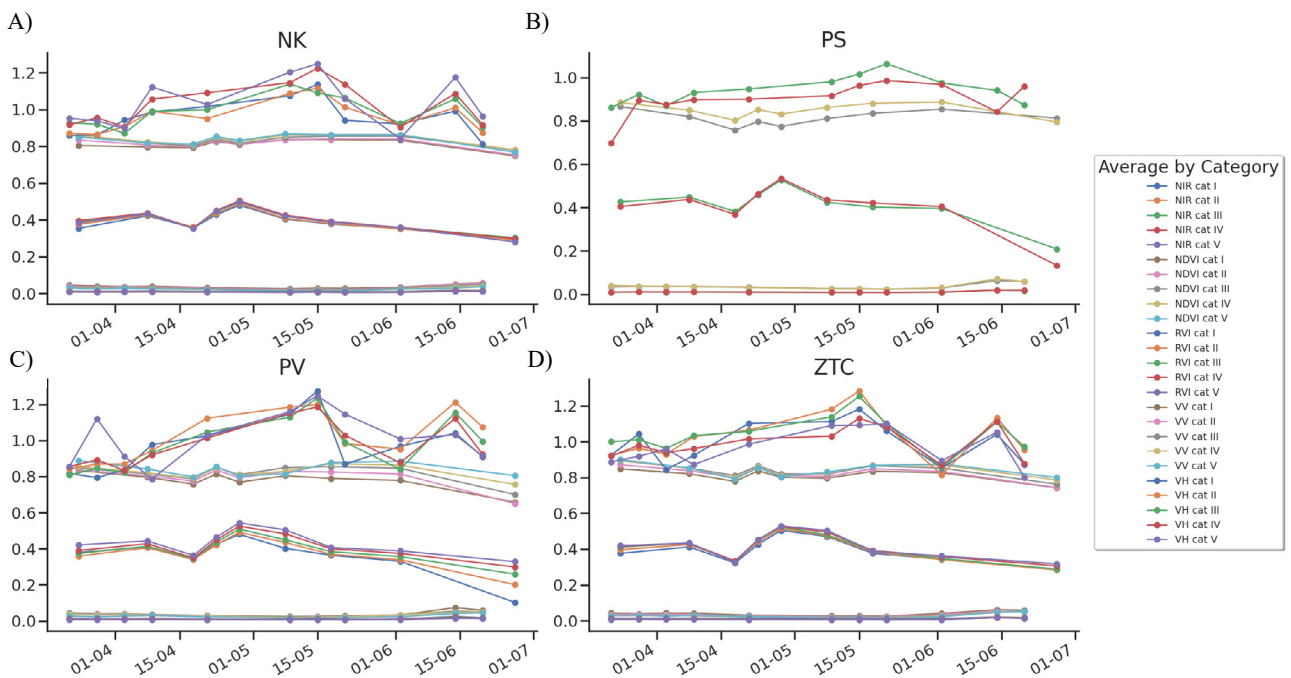


**Fig. 4.** Five MPP (production potential) categories for the given average values of selected variables and plots: NK (A), PS (B), PV (C), ZTC (D) during the main vegetation season 2020 (date on the “x” axis).

model was the small number of training points for the 50 and 100 m resolution. This is not advantageous, for example, for the use of the Random Forest model, which for this reason appeared to us to be inappropriate. A frequently used model for a smaller number of training points is also the support vector machine (SVM). However, the first test indicated that training nonlinear SVM models would be time-consuming, considering the different resolutions.

### 3. RESULTS AND DISCUSSION

#### 3.1. Evaluation of crops in individual zones

Four plots of winter wheat were evaluated using images from the Sentinel 2 satellite: spectral band B8 – a near infrared part of the spectrum to determine the state of plant cell structure (1); the normalized difference vegetation index (NDVI) as an indicator of plant health, structure, and vitality (2); and Sentinel-1: the radar vegetation index (3); and VV and VH polarization (4) as indicators of the state of the wheat stand in terms of biomass growth (its moisture and structure). The variables were evaluated for five MPP classes and three frost-induced damage zones of the monitored plots. Figure 3 shows the average values of the selected variables in the damage zones on the four monitored winter wheat plots. Figure 4 then shows the five MPP categories for the given average values of the variables. The evaluated variables were plotted depending on the date and the BBCH scale (Meier *et al.*, 2009).

RVI clearly showed differences in the damage zones and also between the MPP categories. The lowest RVI values corresponded to the area of the lowest production potential and the greatest damage to the wheat stand. As can be seen from Fig. 2, the places with the most extensive damage to the wheat stand roughly corresponded visually to the places with the lowest production potential. This is a proof that the vegetation in these places is more stressed by abiotic factors and *vice versa*. It can be seen from Fig. 4 that the values between the categories can fluctuate (*e.g.* up to 1.34 for RVI) depending on the current state of the wheat stand in the given phenological phase and according to the damage to the crops induced by frost at the beginning of the main growing season. However, the trend between the categories was maintained. As follows from the literature, SAR data in agriculture was used more for the evaluation of larger areas (*e.g.* Mandal *et al.*, 2020; Saad El Imanni *et al.*, 2022), Bao *et al.*, 2023 and others). Compared to that, our study focuses on the evaluation of smaller units within agricultural plots. These areas can represent, for example, areas of production potential or yield categorization for targeted agrotechnical interventions. Within the course of the RVI curves (Figs 3 and 4), a gradual increase in values with a local maximum (up to 0.95) on March 28 can be observed at the beginning of the monitored period (end of March) of the main vegetation season, which may be associated with the low amount of precipitation during

the end of the tillering growing stage. After that, there is again a gradual decrease in values with a local minimum (up to 0.90) on April 3. From this date, there was a gradual increase in RVI values (up to 1.25) until May 15, as the wheat stand grew during the stem elongation stage and the volume of biomass increased. After that, there was a gradual decrease again, apparently due to phenology and surface structure changes (flowering, ripening). The date June 2, when the local minimum values (up to 0.84) were recorded, corresponded to the flowering growing stage. The application of a fertilizer in the phenological phase of BBCH 32 (2nd node – April 8) proved to be important from the point of view of RVI. After the next application on May 29 (BBCH 59 - end of heading), the values were equalized in terms of RVI (the difference between the categories is on average 0.08), which may have been caused by the uniform maturation of the wheat stand, *i.e.* a change in structure, when the surface of the wheat stand is no longer a green tissue – a leaf, but a maturing ear. Harvest prediction using SAR data was also discussed in the study of Harfenmeister *et al.* (2019), who found an influence of bending of the ears on backscattering. Likewise, Wiseman *et al.* (2014) reported that SAR data can react to dry biomass and can thus unambiguously identify changes in crop structure and phenology, which has proven to be a useful indicator for cereal harvest timing.

The backscatter from cross-polarized channels, for Sentinel-1 VH polarization, is sensitive to structural parameters. For multiple backscatter, the resulting value is high, while for a single backscatter, *e.g.* from bare ground, the resulting value is low. On the other hand, co-polarized channels, with Sentinel-1 VV polarization, are more sensitive to water content or surface roughness (soil, vegetation). Both polarizations clearly showed differences among the categories, while the highest values for both polarizations correspond to the area of the lowest wheat stand quality. The VV polarization reached higher values and was more differentiated according to the degree of damage to the wheat stands (Fig. 3) than the VH polarization. The VH polarization as an expression of surface structure and roughness had a relatively stable, homogeneous course, which pointed to balanced growth during the initial phenological phases (tillering). The increase in values (from 0.019 to 0.042), which probably caused a multiple backscatter, only occurred in the period from the beginning of June, *i.e.* during the phenological phase of flowering and ear formation. This is also where the difference between the damage classes was most noticeable. The VV polarization had a heterogeneous course and greater differences between the classes of crop damage.

For MPP, the VV polarization reached higher values (0.035 on average) at the beginning of the main growing season due to the very low height of the wheat stand in all categories, and at the beginning of growth it was more differentiated than the VH polarization, apparently due to

the different water content in the soil as well, which significantly affects the backscatter. The VH polarization as an expression of the structure (volume) of the surface had a relatively stable, homogeneous course at the beginning of the main growing season, which indicated balanced growth and tillering during the initial phenological phases. The slight increase in values, which was probably caused by a multiple backscatter, already occurred in the period from the beginning of April, *i.e.* at the beginning of stem elongation. In the later phenological phases, there was also a relatively high variability of the VH backscatter among the MPP categories due to the different quality of vegetation on individual parts of the plots. As can be seen from the literature, *e.g.* Harfenmeister *et al.* (2019), Frate *et al.* (2004), Brown *et al.* (2003), and the present results, the VV polarization values decreased with the increase in biomass from 0.035 to 0.006 due to the signal attenuation caused by the development of the vertical plant structure (elongation growth) and the development of the flag leaf. This trend was already visible at the beginning of April. In contrast, the VH polarization was generally more sensitive to the volume (thus structure) of the vegetation and was not as affected by the vertical resolution as the resulting value was inherently affected by the bidirectional scattering (VH) on the plant stem. In the early growth stages, the resulting values were also greatly influenced by changes in the soil moisture of the plots. As confirmed by El Hajj *et al.* (2016), at lower vegetation involvement and height, the signal was significantly affected by the soil contribution. In April and May, the BBCH 30-39 and BBCH 41-49 growth phases began, when both the stem elongation and the flag leaf developed. In these phases, there was also an increase in leaf area coverage up to 100% due to the increase in longer and stronger leaves. In the growth phase of the development of the flag leaf, the values of the VV polarization backscatter usually reached a minimum (0.006). This period is usually characterized by a maximum of leaf area (LAI) values with a high amount of wet biomass, which also dampens the backscatter down to the minimum typical for the given crop. As also confirmed in the study by Hernández *et al.* (2022), VV polarization significantly detects exogenous stress, in this study crop canopy Al stress. In the following growth phase, *i.e.* “heading” (BBCH 51-59), the backscatter values increased again in both polarizations (0.042 for VH and 0.014 for VV), which was mainly caused by a change in the structure of the crop surface. Undoubtedly, the water content in the wheat stands also played a significant role, when in the late phenological phases with decreasing water content and decreasing LAI, the backscatter values also steadily decreased, which is in accordance with the findings of Nasrallah *et al.* (2019). In their study, they mentioned that the VV backscatter was at its lowest value during these late phenological stages.

It follows from the literature (Vreugdenhil *et al.*, 2018; Harfenmeister *et al.*, 2019) that the fluctuations of the backscatter during the growing season can be explained by the changing influence of soil contribution and low vegetation as well as by structural changes of crops and their water content. This is in accordance with our results. Usually, in the early phenological stages, *i.e.* in March, when wheat crops begin to develop tillers (BBCH 20-29), the height of the plants is still low (approx. 10-15 cm) and the growth is not very involved. Thus, soil is still the main factor affecting the backscatter. During this period, the backscatter values were still strongly affected by changes in soil moisture. The backscatter values decreased with the increasing vegetation development due to the higher signal attenuation. This mainly concerned the VV backscatter and was less pronounced for the VH backscatter. The VV backscatter is dominated by the direct contribution of the soil/vegetation combination, where the signal was weakened mainly by the growing vertical parts of the plants (stems). The VH backscatter was generally more sensitive to scatter by the vegetation volume (rather than vertical structure). Double backscattering of VH polarization occurred on the stem. The same development of polarizations during the growth of winter cereals was also mentioned by Vreugdenhil *et al.* (2018). The VV backscatter decreased until the beginning of the stem elongation. The backscatter of VH also decreased slightly during the final tillering stages but increased again with the stem elongation stage due to the increase in the wheat stand volume.

NDVI had a less pronounced curve compared to RVI. The results showed a gradual decrease in NDVI values (from 0.84 to 0.80 on average) for all categories at the beginning of the main growing season. On April 8 (BBCH 32 – 2nd node of stem elongation), fertilizers were applied for the growth and recovery of plants, on April 15 precipitation came, and since April 18 there was a gradual increase in NDVI values (from 0.8 to 0.85). The small fluctuations may have been caused by changes in the structure and vitality of the wheat stand in the individual phenological phases. In terms of damage classes, there is a noticeable fluctuation of values between class 0 and 1, *i.e.* areas with more damage, which is a positive result of the appropriate application of the fertilizer to support plant growth. For MPP, the greatest variability between individual categories was found for the PV and PS plots.

The NIR curve (bands B8 of the Sentinel 2 satellite image) corresponds to the state of the cellular structure of the winter wheat stand. For all four evaluated plots, there was a noticeable increase in reflectance values (from 0.37 to 0.43) at the beginning of April, which was replaced by a decrease due to unfavourable weather (low temperatures) at the beginning of the main growing season. After that, the NIR reflectance values increased again (up to 0.49 on average), which indicates an increase in the volume of biomass during the development of the wheat stand. From the



beginning of May, there was again a gradual decrease in values (from 0.42 to 0.29) related to the change in the growth surface depending on the phenological phase and the structure of the crop tissue. The reflectance values in the NIR fluctuated according to the phenological phase and the state of the cell structure in the given category.

**3.2. Processing and evaluation of remote sensing data**

First, the data used to assess the damage to the wheat crops induced by frost was evaluated. The correlation coefficients showed a positive correlation between the damaged zones, MPP categories, yield, and TWI and a negative correlation with VV, VH, and Slope (see Table 6). The course of crop growth over time, taken into account as a Calendar Day in the model, showed a negligible correlation in all cases. Neither Damaged zones nor MPP Categories are independent of the course of crop growth. The procedure of data resampling from a spatial resolution of 10 to 50 m increased the values of correlation coefficients in most cases, while resampling to 100 m, on the contrary, reduced

it back (sometimes even below its value at a resolution of 10 m). The only exception was the correlation coefficients between damaged zones and MPP, which always decreased when the spatial resolution was reduced.

Regression models (e.g. Lapaz Oliveira *et al.*, 2023) are used to describe the dependencies obtained from radar images, similar to Random Forest machine learning models (Chen *et al.*, 2023; Qu *et al.*, 2023). Because of better results (F-score for Random Forest was 0.528 and for Support Vector Classifier 0.351) and for the reasons stated in section 2.4, we finally decided to use the logistic regression model. In its upper part, Fig. 5 graphically represents the results of building logistic regression. It follows from this part of figure that the built model was able to predict damaged zones with sufficient (1,2) or worse (0) performance.

In terms of performance metrics of the damage zone logistic regression model, the results are shown in Table 7. The precision score, which shows what percentage is truly positive from all positive ones, yielded the best results for the assessed model. However, the F-score, which is the

**Table 6.** Correlation between damage zones and MPP categories and chosen explanatory variables. All coefficients are significant at a 5% significance level

Variables	Damage zones			Variables	MPP Categories		
	Spatial resolution				Spatial resolution		
	10 m	50 m	100 m		10 m	50 m	100 m
TWI	0.135	0.170	0.136	TWI	0.448	0.393	0.573
Yield	0.543	0.590	0.460	Yield	0.369	0.321	0.081
MPP categories	0.557	0.506	0.387	Damage zones	0.557	0.506	0.387
Slope	-0.017	-0.031	-0.022	Slope	-0.271	-0.298	-0.390
VV	-0.226	-0.251	-0.156	VV	-0.200	-0.182	-0.066
VH	-0.186	-0.193	-0.045	VH	-0.221	-0.213	-0.089
Calendar day	-0.000	0.000	-0.000	Calendar day	0.000	0.000	0.000

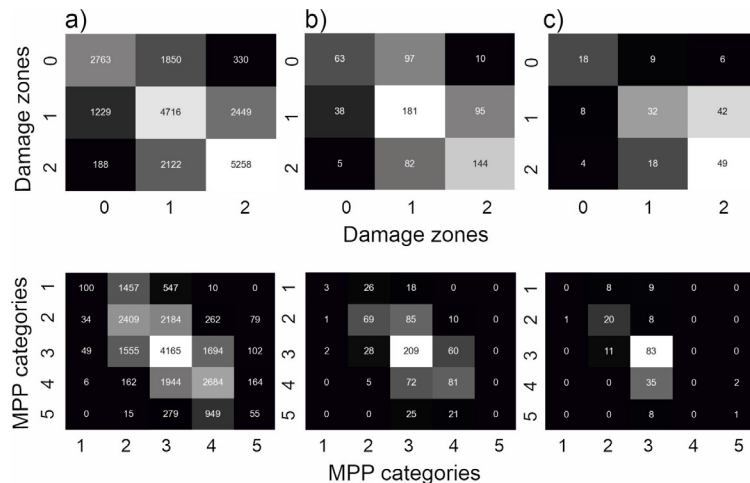


**Fig. 5.** Confusion matrices for logistic regression. a) 10 m data, b) 50 m data, c) 100 m data for damage zones and MPP categories.

**Table 7.** Performance metrics of the built logistic regression models for detection of damaged zones and MPP categories

Parameter	Damage zones			MPP categories		
	10 m	50 m	100 m	10 m	50 m	100 m
F-score	0.611	0.531	0.536	0.323	0.333	0.291
Recall score	0.605	0.523	0.542	0.333	0.338	0.336
Precision score	0.619	0.558	0.549	0.407	0.404	0.285

harmonic mean of precision and recall, still yields a promising result ranging from 0.531 to 0.611, with the best result achieved at a spatial resolution of 10 m.

In the case of evaluation of the MPP categories, the correlation coefficients showed a positive correlation between the MPP categories and damage zones, TWI, and Yield variables and a negative correlation with the Slope, VV, and VH (Table 6). The data resampling procedure sometimes weakened and sometimes strengthened the correlation, while the aforementioned 6 variables were important in the 10 m spatial resolution and for this reason it was chosen.

The results of building logistic regression can be again seen in the lower part of Fig. 5, where the test outcomes are visualized. As can be seen, the built model was able to predict some of the MPP categories with sufficient or worse performance (2, 3 and 4); nevertheless, it seems that other classes are problematic for it (1 and 5).

The performance metrics of the logistic regression model of the MPP categories in the case of F-score showed the best value of 0.333 for the 50 m spatial resolution, the precision score showed the best value at 10 m (0.407), while the recall score showed the best value of 0.338 again at the 50 m spatial resolution.

It is clear from Table 7 that, in the case of evaluation of the MPP categories, the logistic regression model performs slightly better in terms of the F-score, recall, and precision at the smaller resolution (10 and 50 m), compared to the performance at the 100 m resolution. The precision score is the largest of all the monitored performance metrics values at 10 m resolution, indicating that the model is more accurate in its positive predictions, compared to the other resolutions. The F-score value was the best for the 50 m spatial resolution. The recall score indicates that the model's ability to detect positive instances becomes slightly less effective as the resolution decreases. Finally, it could be said that the overall performance (all metrics) decreases as the resolution decreases from 10 to 100 m, suggesting that the model's ability to correctly classify instances diminishes with the smaller resolution.

In terms of comparing both built models, it follows from Table 7 at first glance that the performance metrics were always significantly better for the logistic regression model of damaged zones (the coefficients reached around 0.6 and more in the case of the damage zones and around 0.35 in the case of the MPP categories).

It is clear from the previous statistical analysis that the logistic regression models performed better in the case of a larger spatial resolution (*e.g.* the precision score for the damaged zones was 0.549 for the 100 m spatial resolution, 0.619 for 10 m, and 0.558 for 50 m, see Table 7), with a pixel of 10 m appearing to be the best (in the case of the MPP categories 0.285 for the 100 m spatial resolution, compared to 0.407 for 10 m and 0.404 for 50 m). This is probably due to the fact that, in the case of larger spatial resolutions, more data are available to create a logistic regression model (83 619 for the 10 m spatial resolution against 744 only for 100 m). This is also apparently in accordance with the fact that, in the case of dividing the plots into 3 management zones (frost damage), the results of logistic regression models were better than in the case of dividing them into 5 zones (production potential zones). Based on the results obtained by us, it is perhaps possible to propose an assumption that modern statistical methods can be used to reduce problems associated with radar images speckles for practical purposes. However, confirmation of this finding requires further research.

#### 4. CONCLUSIONS

The results of our experiments proved that the radar data from Sentinel-1 SAR aperture radar has the potential to capture within-field variability in the case of assessing damage to winter wheat plots caused by spring frosts and in the case of assessing their production potential. The radar vegetation index clearly showed differences in damage zones and between production potential categories. The lowest RVI values corresponded to the area of the lowest production potential and the greatest damage to the wheat stand. Also, VH and VV polarizations showed differences among the categories. For both polarizations, the highest values corresponded to the area of the lowest wheat stand quality. The logistic regression model indicated that the larger spatial resolution, with a pixel of 50 m, appeared to be the best in its performance, both in the case of the assessment of damaged zones and MPP categories. It was predominantly true that the greater spatial resolution was more effective for its use. In the case of assessing damage to winter wheat stands caused by spring frosts, correlation coefficients of up to 0.7 were reached. Modern statistical methods can probably be used to reduce problems associated with speckles of radar images for practical purposes, but confirmation of this finding requires further research.

**Acknowledgments:** We would like to thank to the management of agriculture company Lupofyt for providing agronomic data.

**Conflict of interest:** The authors declare that they have no conflict of interest.

**Data availability:** The data used for this paper is available upon request from the corresponding author. The data used in this study were downloaded from the Copernicus Open Access Hub and Czech Cadastre.

## 5. REFERENCES

- Atzberger, C., 2013. Advances in remote sensing of agriculture: context description, existing operational monitoring systems and major information needs. *Remote Sensing* 5, 949-981. <https://doi.org/10.3390/rs5084124>
- Balázsová, K., Chyba, J., Kumhálová, J., Mašek, J., Petrásěk, S., 2021. Monitoring of Khorasan (*Triticum turgidum* ssp. *Turanicum*) and modern kabot spring wheat (*Triticum aestivum*) varieties by UAV and sensor technologies under different soil tillage. *Agronomy* 11(7), 1348. <https://doi.org/10.3390/agronomy11071348>
- Bao, X., Zhang, R., Lv, J., Wu, R., Zhang, H., Chen, J., *et al.*, 2023. Vegetation descriptors from Sentinel-1 SAR data for crop growth monitoring. *ISPRS J. Photogrammetry Remote Sensing* 203, 86-114. <https://doi.org/10.1016/j.isprsjprs.2023.07.023>
- Barlow, K.M., Christy, B.P., O'Leary, G.J., Riffkin, P.A., Nuttall, J.G., 2015. Simulating the impact of extreme heat and frost events on wheat crop production: A review. *Field Crops Res.* <https://doi.org/10.1016/j.fcr.2014.11.010>
- Brown, S.C.M., Quegan, S., Morrison, K., Bennett, J.C., Cookmartin, G., 2003. High-resolution measurements of scattering in wheat canopies-implications for crop parameter retrieval. *IEEE Transactions on Geoscience and Remote Sensing* 41, 1602-1610. <https://doi.org/10.1109/TGRS.2003.814132>
- Challinor, A.J., Wheeler, T.R., Craufurd, P.Q., Slingo, J.M., 2005. Simulation of the impact of high temperature stress on annual crop yields. *Agric. Meteorol.* 135, 180-189. <https://doi.org/10.1016/j.agrformet.2005.11.015>
- Charbonneau, F., Trudel, M., Fernandes, R., 2005. Use of dual polarization and multi-incidence SAR for soil permeability mapping. Proc. 2005 Advanced Synthetic Aperture Radar (ASAR) workshop, St-Hubert, QC, Canada.
- Chen, D., Hu, H., Liao, C., Ye, J., Bao, W., Mo, J., *et al.*, 2023. Crop NDVI time series construction by fusing Sentinel-1, Sentinel-2, and environmental data with an ensemble-based framework. *Comput. Electron. Agric.* 215. <https://doi.org/10.1016/j.compag.2023.108388>
- Dalmanndottir, S., Jørgensen, M., Rapacz, M., Østrem, L., Larsen, A., Rødven, R., *et al.*, 2017. Cold acclimation in warmer extended autumns impairs freezing tolerance of perennial ryegrass (*Lolium perenne*) and timothy (*Phleum pratense*). *Physiol. Plant.* 160, 266-281. <https://doi.org/10.1111/ppl.12548>
- de Blas, C.S., Valcarce-Diñeiro, R., Sipols, A.E., Sánchez Martín, N., Arias-Pérez, B., Santos-Martín, M.T., 2021. Prediction of crop biophysical variables with panel data techniques and radar remote sensing imagery. *Biosyst. Eng.* 205, 76-92. <https://doi.org/10.1016/j.biosystemseng.2021.02.014>
- Domínguez, J.A., Kumhálová, J., Novák, P., 2015. Winter oilseed rape and winter wheat growth prediction using remote sensing methods. 61, 410-416. <https://doi.org/10.17221/412/2015-PSE>
- El Hajj, M., Baghdadi, N., Zribi, M., Belaud, G., Cheviron, B., Courault, D., *et al.*, 2016. Soil moisture retrieval over irrigated grassland using X-band SAR data. *Remote Sens. Environ.* 176, 202-218. <https://doi.org/10.1016/j.rse.2016.01.027>
- ESA - Copernicus [WWW Document], n.d. URL [https://www.esa.int/Applications/Observing\\_the\\_Earth/Copernicus](https://www.esa.int/Applications/Observing_the_Earth/Copernicus) (accessed 4.2.24).
- Evans, L.T., 1996. Crop evolution, adaptation and yield. Cambridge University Press, UK, ISBN 0-521-29588-0, 500 pp.
- Fieuzal, R., Baup, F., Marais-Sicre, C., 2013. Monitoring wheat and rapeseed by using synchronous optical and radar satellite data-from temporal signatures to crop parameters estimation. *ARS* 02, 162-180. <https://doi.org/10.4236/ars.2013.22020>
- Filippini, F., 2019. Sentinel-1 GRD Preprocessing Workflow. *Proceedings* 18, 11-18. <https://doi.org/10.3390/ECRS-3-06201>
- Fowler, D.B., Limin, A.E., Ritchie, J.T., 1999. Low-Temperature tolerance in cereals: Model and genetic interpretation. *Crop Sci.* 39, 626-633. <https://doi.org/10.2135/cropsci1999.0011183X003900020002x>
- Frate, F. Del, Ferrazzoli, P., Guerriero, L., Strozzi, T., Wegmuller, U., Cookmartin, G., *et al.*, 2004. Wheat cycle monitoring using radar data and a neural network trained by a model. *IEEE Trans. Geosci. Remote Sensing* 42, 35-44. <https://doi.org/10.1109/TGRS.2003.817200>
- Fuglie, K., 2021. Climate change upsets agriculture. *Nature Climate Change* 2021 11:4 11, 294-295. <https://doi.org/10.1038/s41558-021-01017-6>
- Gao, Y., Pan, Y., Zhu, X., Li, L., Ren, S., Zhao, C., *et al.*, 2023. FARM: A fully automated rice mapping framework combining Sentinel-1 SAR and Sentinel-2 multi-temporal imagery. *Comput. Electron. Agric.* 213. <https://doi.org/10.1016/j.compag.2023.108262>
- Guilpart, N., Grassini, P., Sadras, V.O., Timsina, J., Cassman, K.G., 2017. Estimating yield gaps at the cropping system level. *Field Crops Res.* 206, 21-32. <https://doi.org/10.1016/j.fcr.2017.02.008>
- Harfenmeister, K., Spengler, D., Weltzien, C., 2019. Analyzing temporal and spatial characteristics of crop parameters using sentinel-1 backscatter data. *Remote Sensing* 11, 1569. <https://doi.org/10.3390/rs11131569>
- Hernández, M., Borges, A.A., Francisco-Bethencourt, D., 2022. Mapping stressed wheat plants by soil aluminum effect using C-band SAR images: implications for plant growth and grain quality. *Precis. Agric.* 23, 1072-1092. <https://doi.org/10.1007/s11119-022-09875-6>
- Jelínek, Z., Kumhálová, J., Chyba, J., Wohlmuthová, M., Madaras, M., Kumhála, F., 2020. Landsat and Sentinel-2 images as

- a tool for the effective estimation of winter and spring cultivar growth and yield prediction in the Czech Republic. *Int. Agrophys.* 34, 391-406. <https://doi.org/10.31545/intagr/126593>
- Jin, X., Yang, G., Xu, X., Yang, H., Feng, H., Li, Z., *et al.*, 2015. Combined multi-temporal optical and radar parameters for estimating LAI and biomass in winter wheat using HJ and RADARSAR-2 Data. *Remote Sensing* 7, 13251-13272. <https://doi.org/10.3390/rs71013251>
- Kajla, M., Yadav, V.K., Khokhar, J., Singh, S., Chhokar, R.S., Meena, R.P., *et al.*, 2015. Increase in wheat production through management of abiotic stresses: A review. *J. Appl. Natural Sci.* 7, 1070-1080. <https://doi.org/10.31018/jans.v7i2.733>
- Kaplan, G., Fine, L., Lukyanov, V., Manivasagam, V.S., Tanny, J., Rozenstein, O., 2021. Normalizing the local incidence angle in sentinel-1 imagery to improve leaf area index, vegetation height, and crop coefficient estimations. *Land (Basel)* 10, 680. <https://doi.org/10.3390/land10070680>
- Kim, Y., Jackson, T., Bindlish, R., Lee, H., Hong, S., 2012. Radar vegetation index for estimating the vegetation water content of rice and soybean. *IEEE Geoscience and Remote Sensing Letters* 9, 564-568. <https://doi.org/10.1109/LGRS.2011.2174772>
- Kumar Sahadevan, D., Rao Sitiraju, S., Dinesh Kumar, S., Srinivasa Rao, S., Sharma, J.R., 2013. Radar Vegetation Index as an Alternative to NDVI for Monitoring of Soyabean and Cotton, Indian Cartographer
- Kumhálová, J., Kumhála, F., Kroulík, M., Matějková, Š., 2011. The impact of topography on soil properties and yield and the effects of weather conditions. *Precis. Agric.* 12, 813-830. <https://doi.org/10.1007/s11119-011-9221-x>
- Kumhálová, J., Kumhála, F., Novák, P., Matějková, Š., 2013. Airborne laser scanning data as a source of field topographical characteristics. <https://pse.agriculturejournals.cz/doi/10.17221/188/2013-PSE.html> 59, 423-431. <https://doi.org/10.17221/188/2013-PSE>
- Kumhálová, J., Zemek, F., Novák, P., Brovkina, O., Mayerová, M., 2014. Use of Landsat images for yield evaluation within a small plot. *Plant Soil Environ.* 60, 501-506. <https://doi.org/10.17221/515/2014-PSE>
- Landsat Science [WWW Document], n.d. URL <https://landsat.gsfc.nasa.gov/> (accessed 4.2.24).
- Lapaz Oliveira, A.M., Castro-Franco, M., Saínz Rozas, H.R., Carciocchi, W.D., Balzarini, M., Avila, O., *et al.*, 2023. Monitoring corn nitrogen nutrition index from optical and synthetic aperture radar satellite data and soil available nitrogen. *Precis. Agric.* 24, 2592-2606. <https://doi.org/10.1007/s11119-023-10054-4>
- Madaras, M., Mayerová, M., Kumhálová, J., Lipavská, J., 2018. The influence of mineral fertilisers, farmyard manure, liming and sowing rate on winter wheat grain yields. *Plant Soil Environ.* 64, 38-46. <https://doi.org/10.17221/703/2017-PSE>
- Malenovský, Z., Rott, H., Cihlar, J., Schaepman, M.E., García-Santos, G., Fernandes, R., *et al.*, 2012. Sentinels for science: Potential of Sentinel-1, -2, and -3 missions for scientific observations of ocean, cryosphere, and land. *Remote Sens. Environ.* 120, 91-101. <https://doi.org/10.1016/j.rse.2011.09.026>
- Mandal, D., Kumar, V., Ratha, D., Dey, S., Bhattacharya, A., Lopez-Sanchez, J.M., *et al.*, 2020. Dual polarimetric radar vegetation index for crop growth monitoring using sentinel-1 SAR data. *Remote Sens Environ.* 247, 111954. <https://doi.org/10.1016/j.rse.2020.111954>
- Maphanyane, J.G., Mapeo, R.B., Akinola, M.O., (Eds), 2018. Handbook of Research on Geospatial Science and Technologies. IGI Global. <https://doi.org/10.4018/978-1-5225-3440-2>
- Meier, U., Bleiholder, H., Buhr, L., Feller, C., Hack, H., Heß, M., *et al.*, 2009. Das BBCH-System zur Codierung der phänologischen Entwicklungsstadien von Pflanzen-Geschichte und Veröffentlichungen, J. Kulturpflanzen.
- Moreira, A., Prats-Iraola, P., Younis, M., Krieger, G., Hajnsek, I., Papathanassiou, K.P., 2013. A tutorial on synthetic aperture radar. *IEEE Geosci. Remote Sens. Mag.* 1, 6-43. <https://doi.org/10.1109/MGRS.2013.2248301>
- Nasrallah, A., Baghdadi, N., El Hajj, M., Darwish, T., Belhouchette, H., Faour, G., *et al.*, 2019. Sentinel-1 data for winter wheat phenology monitoring and mapping. *Remote Sensing (Basel)* 11. <https://doi.org/10.3390/rs11192228>
- Nasrallah, A., Baghdadi, N., Mhawej, M., Faour, G., Darwish, T., Belhouchette, H., *et al.*, 2018. A Novel approach for mapping wheat areas using high resolution sentinel-2 images. *Sensors* 2018, 18, 2089. <https://doi.org/10.3390/s18072089>
- Oerke, E.-C., 1994. Crop production and crop protection: estimated losses in major food and cash crops. Elsevier.
- Persson, T., Bergjord Olsen, A.K., Nkurunziza, L., Sindhøj, E., Eckersten, H., 2017. Estimation of crown temperature of winter wheat and the effect on simulation of frost tolerance. *J. Agron. Crop Sci.* 203, 161-176. <https://doi.org/10.1111/jac.12187>
- Qu, X., Zhou, J., Gu, X., Wang, Y., Sun, Q., Pan, Y., 2023. Monitoring maize lodging severity based on multi-temporal Sentinel-1 images using time-weighted dynamic time warping. *Comput. Electron. Agric.* 215. <https://doi.org/10.1016/j.compag.2023.108365>
- Rapacz, M., Ergon, A., Höglind, M., Jørgensen, M., Jurczyk, B., Østrem, L., *et al.*, 2014. Overwintering of herbaceous plants in a changing climate. Still more questions than answers. *Plant Sci.* 225, 34-44. <https://doi.org/10.1016/j.plantsci.2014.05.009>
- Rapacz, M., Macko-Podgórní, A., Jurczyk, B., Kuchar, L., 2022. Modeling wheat and triticale winter hardiness under current and predicted winter scenarios for Central Europe: A focus on deacclimation. *Agric. Meteorol.* 313. <https://doi.org/10.1016/j.agrformet.2021.108739>
- Rataj, V., Kumhálová, J., Macák, M., Barát, M., Galambošová, J., Chyba, J., *et al.*, 2022. Long-term monitoring of different field traffic management practices in cereals production with support of satellite images and yield data in context of climate change. *Agronomy* 12, 128. <https://doi.org/10.3390/agronomy12010128>
- Rouse, J., Haas, R.H., Schell, J.A., Deering, D., 1973. Monitoring vegetation systems in the great plains with ERTS.
- Saad El Imanni, H., El Harti, A., Panimboza, J., 2022. Investigating Sentinel-1 and Sentinel-2 data efficiency in studying the temporal behavior of wheat phenological stages using google Earth engine. *Agriculture* 12, 1605. <https://doi.org/10.3390/agriculture12101605>

- Sánchez, B., Rasmussen, A., Porter, J.R., 2014. Temperatures and the growth and development of maize and rice: a review. *Glob. Chang. Biol.* 20, 408-417. <https://doi.org/10.1111/gcb.12389>
- Šíp, V., Chrpová, J., Žofajová, A., Milec, Z., Mihalik, D., Pánková, K., *et al.*, 2011. Evidence of selective changes in winter wheat in middle-European environments reflected by allelic diversity at loci affecting plant height and photoperiodic response. *J. Agric. Sci.* 149, 313-326. <https://doi.org/10.1017/S002185961000078X>
- Special Report on Climate Change and Land - IPCC site [WWW Document], n.d. . [https://reliefweb.int/sites/reliefweb.int/files/resources/4.-SPM\\_Approved\\_Microsite\\_FINAL.pdf](https://reliefweb.int/sites/reliefweb.int/files/resources/4.-SPM_Approved_Microsite_FINAL.pdf). URL <https://www.ipcc.ch/srccl/> (accessed 4.2.24).
- Thielert, W., 2006. A unique product: The story of the imidacloprid stress shield. *Pflanzenschutz-Nachr. Bayer* 59, 73-86. <https://doi.org/10.1097/01.HJ.0000286495.86766.a7>
- Trudel, M., Charbonneau, F., Leconte, R., 2012. Using RADARSAT-2 polarimetric and ENVISAT-ASAR dual-polarization data for estimating soil moisture over agricultural fields. *Canadian J. Remote Sensing* 38, 514-527.
- Tůma, L., Kumhálová, J., Kumhála, F., Krepl, V., 2022. The noise-reduction potential of radar vegetation index for crop management in the Czech Republic. *Precis. Agric.* 23, 450-469. <https://doi.org/10.1007/s11119-021-09844-5>
- Vaghela, B.N., Solanki, H.A., Kalubarme, M.H., 2020. Winter wheat growth assessment using temporal normalized phenology index (TNPI) in Bhuj Taluka, Gujarat State, India. *Remote Sens. Appl.* 20. <https://doi.org/10.1016/j.rsase.2020.100422>
- Vreugdenhil, M., Wagner, W., Bauer-Marschallinger, B., Pfeil, I., Teubner, I., Rüdiger, C., Strauss, P., 2018. Sensitivity of Sentinel-1 backscatter to vegetation dynamics: An Austrian case study. *Remote Sensing (Basel)* 10. <https://doi.org/10.3390/rs10091396>
- Wiseman, G., McNairn, H., Homayouni, S., Shang, J., 2014. RADARSAT-2 polarimetric sar response to crop biomass for agricultural production monitoring. *IEEE J. Sel. Top Appl. Earth Obs. Remote Sens.* 7, 4461-4471. <https://doi.org/10.1109/JSTARS.2014.2322311>
- WMS – Climatic regions of the Czech Republic: <https://micka.cenia.cz/record/basic/4e64bc59-65b0-4475-aae2-06a8c0a80138> . Accessed: 13.2.2024.
- Ya'nan, Z.H.O.U., Binyao, W.A.N.G., Weiwei, Z.H.U., Li, F.E.N.G., Qisheng, H.E., Xin, Z., *et al.*, 2024. Spatial-temporal constraints for surface soil moisture mapping using Sentinel-1 and Sentinel-2 data over agricultural regions. *Comput. Electron. Agric.* 219. <https://doi.org/10.1016/j.compag.2024.108835>
- Zhong, X., Mei, X., Li, Y., Yoshida, H., Zhao, P., Wang, X., *et al.*, 2008. Changes in frost resistance of wheat young ears with development during jointing stage. *J. Agron. Crop. Sci.* 194, 343-349. <https://doi.org/10.1111/j.1439-037X.2008.00320.x>